Structure of the Inhibitor W7 Bound to the Regulatory Domain of Cardiac Troponin C[†]

Ryan M. B. Hoffman and Brian D. Sykes*

Department of Biochemistry, University of Alberta, Edmonton, Alberta, Canada T6G 2H7

Received February 4, 2009; Revised Manuscript Received May 2, 2009

ABSTRACT: The calmodulin antagonist W7 binds to troponin C in the presence of Ca^{2+} and inhibits striated muscle contraction. This study integrates multiple data into the structure of the regulatory domain of human cardiac troponin C (cNTnC) bound to Ca^{2+} and W7. The protein−W7 interface is defined through a three-dimensional $\{^1H,^{13}C\}$-edited-$\{^1H,^{12}C\}$-detected NOESY NMR experiment, and other aspects of the structure are modeled as perturbations to previously known coordinates and restraints. The structure determination protocol optimizes the protein−W7 contacts prior to the introduction of protein−W7 steric interactions or conformational changes in the protein. The structure determination protocol gives families of conformers that all have an optimal docking as assessed by satisfaction of the target function. The structure supports the previously proposed troponin I blocking mechanism for the activity of W7 in striated muscle and suggests a role for the flexible tail of W7 in stabilization of the bound state. This clarifies the structure−activity relationships of W7 and implicates an electrostatically mediated component of activity in common analogues of W7, including the antipsychotic trifluoroperazine and the cardiotonic levosimendan.

High-quality protein structural models offer new insights into biochemical mechanisms and new points of departure for experimentation. Each protein crystal represents not only a possible protein X-ray structure but also a host of potential protein−ligand costructures. If ligand binding does not cause a large perturbation to the conformation of the protein, the costructures can be obtained by soaking the previously determined crystal in mother liquor containing the ligand. The high solvent content of protein crystals allows the ligand to penetrate the lattice and bind to the protein. If the resulting crystals are isomorphous to the previously determined one, the structure and location of the ligand can be determined from a difference Fourier map which is easy compared with the determination of a new X-ray structure from scratch.

NMR[1] data can be easily acquired for a panel of homologous protein·ligand complexes. However, there is no widely used NMR approach similar to the crystallographic methodology of crystal soaking and model building through a difference Fourier map, bootstrapping the determination of a protein−ligand structure through the assumption of a small perturbation to a known one. This is unusual since NMR provides so many structurally correlated observations; even a simple titration experiment can directly show the magnitude and nature of a binding-induced perturbation. One popular docking protocol using minimal information is HADDOCK (High Ambiguity Driven protein−protein DOCKing) (*1*). This algorithm is used for the structure determination of complexes of biomolecules (proteins and nucleic acids) with known structures. HADDOCK can incorporate highly ambiguous information such as titration-monitored chemical shift perturbations and can be used to contrast scenarios where unambiguous knowledge (like intermolecular NOEs) is used for structure determination (*1*).

We sought a HADDOCK-like protocol appropriate for the docking of druglike molecules to structures previously determined by our own group, more closely akin to the crystallographic approach. Our research has described the conformation of the regulatory N-terminal domain of human cardiac troponin C in three biological states [off, on, and bound to cNTnC·Ca^{2+}'s biological target, a region of troponin I called the switch peptide (Sp)] and one chemotherapeutic state (bound to Sp and bepridil) (*2−4*). Each of those studies represents a unique structure determination, even though the structures are all highly similar to each other. Similarly, Ikura and co-workers determined the calmodulin NMR structure (*5*) and then determined the structure again in the presence of the model ligand W7 (*6*).

Previous work has shown that W7, a known inhibitor of striated muscle contraction, targets TnC in the muscle fiber (*7*). The proposed mechanism has W7 binding to the calcium-bound N-terminal domain of human cardiac troponin C (cNTnC·Ca^{2+})

---

*To whom correspondence should be addressed: Room 4-70, Medical Sciences Bldg., University of Alberta, Edmonton, Alberta, Canada T6G 2H7. Phone: (780) 492-5460. Fax: (780) 492-0886. E-mail: brian.sykes@ualberta.ca.

[1]Abbreviations: cNTnC, N-terminal domain of human cardiac troponin C (C35S, C84S, residues 1−89); NMR, nuclear magnetic resonance (spectroscopy); Sp, switch region of human cardiac troponin I (residues 147−163); K_d, dissociation constant.

and interfering with the association of cNTnC·Ca^{2+} with Sp. This makes the cNTnC·Ca^{2+}−W7 equilibrium an attractive model system for the development of drugs that modulate cardiac contraction (*8*). NMR studies have shown that W7 binds to cNTnC·Ca^{2+} and effects the biologically pivotal closed-to-open conformational transition (*9, 10*). W7 binding can occur in the presence of Sp, albeit anticooperatively (*10*). All of these observations are in accord with previous results on the cNTnC·Ca^{2+}−bepridil system (*4*). As the Ca^{2+} dependence of the TnC−W7 interaction is independently known (*11*), the conformational transition resulting from binding is independently character-ized (*9, 10*), and the coordinates of analogous protein−ligand complexes are known (*4*), we sought to bootstrap a cNTnC·Ca^{2+}·W7 structure determination using the previous knowledge, analogous to the crystallographic approach using crystal soaks and difference Fourier maps.

Our early attempts to describe the structure of W7 bound to cNTnC·Ca^{2+} focused on the characterization of the solution equilibrium. Although 41 backbone amide {^{1}H,^{15}N}-HSQC signals monitored during a W7 titration could be fit to a single-site binding model, numerous side chain methyl {^{1}H,^{13}C}-HSQC signals reflected a secondary binding process (*9*). Attempts to derive a structure of the cNTnC·Ca^{2+}·W7 complex were confounded by multiple binding sites and/or the presence of multiple docked poses (*12*). This latter complication was also identified in the highly analogous calmodulin−J8 system (*13*). In this study, we circumvent these difficulties by studying a 1:1 complex and using a filtered, edited NOESY experiment to assign specific intermolecular contacts.

As W7 binding induced conformational changes in cNTnC·Ca^{2+} that were similar (as monitored by NMR) to those induced by the binding of Sp (*9, 10*), we investigate the assumption that the distance restraints used to define the protein conformation can be reused from the study defining the structure of the cNTnC·Ca^{2+}·Sp complex. We propose that the obligatory data toward defining the protein−ligand complex are the actual contacts between cNTnC·Ca^{2+} and W7. As calcium binding is a known prerequisite for binding, as the protein conformation is to be approximated from analogous structures, and as the protein−W7 contacts can be precisely and accurately known (from experimental data presented here), a structure determina-tion blending these different data must correctly weight their relative information contents. So in this paper we incorporate multiple independently procured lines of evidence toward the structure of cNTnC·Ca^{2+}·W7. The structure supports a Sp blocking mechanism for the activity of W7 in striated muscle and helps elucidate the role of the flexible tail of W7 in binding.

MATERIALS AND METHODS

Reagents. The cloning, mutagenesis, and expression of the N-terminal domain of human cardiac TnC (C35S, C84S, residues 1−89) have been reported previously (*14*). W7 [*N*-(6-aminohex-enyl)-5-chloronaphthalenesulfonamide] was purchased from Sigma-Aldrich as a hydrochloride salt. Calcium chloride (Sigma-Aldrich) and DSS-d_6 (Chenomx Inc.) were purchased as analytical-grade stock solutions. Other reagents were prepara-tion-grade. Isotopic labels were purchased from Cambridge Isotope Laboratories.

Assignment of W7. The NMR spectrum of W7 in DMSO-d_6 at 30 °C was assigned using natural abundance ^{1}H and ^{13}C spectra acquired on a 10 mM sample on a four-channel Varian

600 MHz NMR Inova spectrometer with a Z-pulsed field gradient probe, or a 215 mM sample on a Varian Inova 800 MHz spectrometer equipped with a Z-gradient HCN 5 mm "cold probe". The acquisition parameters at 600 MHz were as follows: {^{1}H,^{13}C}-HMBC, 8000 Hz spectral width in the directly detected (^{1}H) dimension (sw), 2200 Hz spectral width in the indirect (^{13}C) dimension (sw1), 61 ms acquisition time (at), 144 indirectly detected points (ni), and the carbon−proton scalar coupling set to 165 Hz; {^{1}H,^{13}C}-HSQC, sw = 8000 Hz, sw1 = 2200 Hz, at = 61 ms, ni = 144, and jCH = 143 Hz; {^{1}H,^{1}H}-DQF-COSY, sw = 8000 Hz, sw1 = 8000 Hz, at = 256 ms, and ni = 512; one-dimensional ^{1}H, sw = 8000 Hz, and at = 4.0s; one-dimensional ^{13}C, sw = 20000 Hz, and at = 0.5 s, with broadband Waltz16 decoupling. The sample was not spun. Acquisition parameters at 800 MHz for one-dimensional ^{13}C were sw = 5000 Hz (centered on the aromatic region) and at = 4.0 s, with Waltz16 ^{1}H decoupling and sample spinning. All NMR experiments were conducted in Biopack using VnmrJ 2.1B (Varian Inc.).

Titration Studies. Concentrations were determined gravime-trically to a precision of ±0.05 mg. Initially, the buffer was comprised of 100 mM KCl, 10 mM imidazole, DSS-d_6 (83 μM), CaCl$_2$ (4.9 mM), and W7 (1.5 mM) in D$_2$O. Immediately before the titration experiments, 0.5 μL of 1 M imidazole equilibrated in H$_2$O was added to the 500 μL NMR sample to provide an internal pH reference (*15*). Protein was titrated into the W7 solution either as a dry powder (titration 1) or as a buffered stock solution (titration 2). For titration 1, the initial pH (technically a pD as the solvent is D$_2$O) was adjusted to 6.8.

Weighed amounts of lyophilized cNTnC were transferred to the W7 solution. Significant pH corrections were required over the titration as the lyophilized protein is acidic. Resultant changes in pH were detected by ^{1}H NMR spectra (*15*) and were corrected through additions of 0.1−1 M NaOD or DCl. At each pH-corrected increment, ^{1}H NMR spectra were acquired, including a T_1 relaxation series (see below). For titration 2, the initial pH of the NMR sample was adjusted to 6.8. A stock 2.0 mM cNTnC solution was prepared under matched conditions. The pH was adjusted to a range of 6.5−7.0, measured with pH paper; 10 μL increments of protein were added to the sample at each titration point, and small aliquots of acid or base were added to maintain a constant pH.

Titrations were monitored using one-dimensional ^{1}H NMR (600 MHz) spectra acquired at 30 °C. The samples were not spun. Spectra were processed with NMRPipe/NMRDraw (*16*). Proces-sing featured mild apodization and zero filling prior to Fourier transformation in both dimensions, and forward-back linear prediction in the indirect dimension. The spectra were referenced internally to the DSS signal. Peak picking and analysis was performed with the NANUC distribution of NMRView (*17*) as maintained by P. Mercier (Chenomx Inc.). Increments of titra-tion 1 (above) were also monitored with ^{1}H T_1 relaxation series. The "water" experiment of BioPack was used, with an initial equilibration delay (d_1) of 2.5 s, and a 4.0 s acquisition. A 180° pulse (15.6 ms) was followed by a variable relaxation delay (d_2) and a readout pulse. The relaxation delay was incremented as follows: 0.01, 0.0225, 0.0508, 0.1145, 0.2580, 0.5814, 1.3104, 2.9532, 6.6557, and 15 s (an exponentially distributed sampling, generated with the Parameter Arrays submenu of VnmrJ 2.1B). Spectra were processed with 0.5 Hz exponential line broadening in VnmrJ; relaxation analysis was performed within that pro-gram. Peak intensities were quantified with drift correction using the macro "fpdc". The data were fit and visualized with the

Table 1: Chemical Shifts of W7 in the Free State in NMR Buffer and T_1 Relaxation Times of the W7 Protons Free and in the Presence of 18% (molar ratio) cNTnC·Ca^{2+}·W7 Complex[a]

		T_1 (s)	
signal	shift (ppm)	free W7	18% (molar ratio) cNTnC·Ca^{2+}·W7
H2	8.34	3.45 ± 0.105	1.53 ± 0.063
H3	7.80	2.37 ± 0.055	1.56 ± 0.066[b]
H4	8.58	3.02 ± 0.061	1.60 ± 0.092
H6	7.87	3.77 ± 0.071	1.56 ± 0.066[b]
H7	7.72	2.36 ± 0.050	1.59 ± 0.072
H8	8.70	3.48 ± 0.075	1.56 ± 0.094
H11	2.95	0.804 ± 0.007	0.850 ± 0.029
H12	1.24	0.895 ± 0.032	1.04 ± 0.095[b]
H13/14	0.97	0.921 ± 0.015	0.896 ± 0.048
H15	1.30	1.21 ± 0.029	1.04 ± 0.095[b]
H16	2.75	1.54 ± 0.021	1.04 ± 0.017

[a] Note that signals H11−H16 correspond to two methylene protons. [b] T_1 values correspond to more than one signal due to spectral overlap.

commands "t1 expl" (Figure Supp-1 of the Supporting Information). The multiple *J*-coupled lines corresponding to an individual signal were averaged along with their errors. This procedure was performed for free W7 in buffer (titration increment 0) and for W7 in the presence of 18% (molar ratio) cNTnC·Ca^{2+} (titration increment 2; see Table 1).

Intermolecular NOEs. A 1:1 complex was prepared under the same solution conditions that were used for the binding experiments (100 mM KCl, 10 mM imidazole, 83 μM DSS-d_6, and 4.9 mM CaCl$_2$); 2.7 mg of lyophilized {^{13}C,^{15}N}-enriched cNTnC and 0.2 mg of W7 were dissolved in a final volume of 550 μL to generate ~0.8 mM 1:1 complex.

Intermolecular NOEs were obtained using a three-dimensional, {^{1}H,^{13}C}-edited, ^{12}C-filtered, transferred NOESY experiment (18) included in Biopack (Varian Inc.). A chief advantage of this pulse sequence is that the directly detected dimension does not require ^{13}C decoupling, allowing long acquisition times and therefore higher digital resolution. The three-dimensional (3D) spectrum was acquired at 800 MHz with sweep widths of 8000 Hz in the directly detected (W7) dimension, 8000 Hz in the indirect (protein) dimension, and 4022 Hz in the indirect (protein ^{13}C) dimension. There were 2048, 160, and 64 complex points acquired in the direct ^{1}H, indirect ^{1}H, and indirect ^{13}C dimensions, respectively. The data were processed with NMRPipe (16). Strong apodization was required because the long acquisition time resulted in too much incorporation of noise into the indirectly detected dimensions. The direct dimension was apodized with an unshifted squared cosine function, and a 5 Hz line broadening was imposed with an exponential window. Forward-back linear prediction was used in the indirect dimensions. Spectral assignment was facilitated with NMRView and NMRViewJ. Titration data and assignments from previous studies (9, 10) were also used to interpret the intermolecular NOE data. Strip plots of the assigned contacts are shown in Figure 5. The assigned methyl groups involved in the 31 protein−ligand contacts are highlighted in Figure Supp-2 of the Supporting Information. Each assigned NOE was interpreted as a contact without further interpretation of the significance of peak intensities. One reason for this strategy is that it avoids the problems inherent in calibrating NOE intensities in the presence of chemical exchange.

NOE Target Functions. There are three classes of NOE data used in this study corresponding to various degrees of inductive support. For example, W7 binds only to calcium-saturated cNTnC (11), so the distance restraints defining the protein−Ca^{2+} interactions [pseudo-NOEs derived from crystal structures (2)] were given a scaling of 1000. The calcium ion remains docked over the entire simulation, and so the magnitude of its scaling does little to alter the convergence of the calculation, except to ensure that these restraints are not violated. In contrast, the intraprotein NOE data are taken from the structure determination of Protein Data Bank (PDB) entry 1MXL (cNTnC·Ca^{2+}·Sp, reflecting the open conformation) where the calibration of the restraints was highly precise. As described below, the optimal docking solution does require some conformational changes in the protein, so the intraprotein restraints needed to be deweighted in favor of the more pertinent data. As such, the intraprotein restraints were defined with a default scaling of 1. The most informative restraints, those derived from the cNTnC·Ca^{2+}−W7 NOEs in this study, were applied with a scaling of 10 so that they would dominate the intraprotein restraints in the calculation. They were all calibrated between the same distance bounds (1.8 and 5 Å) and were applied with "hard" (quadratic) scaling at their extrema. NMR assignments and distance restraints are available at the Biological Magnetic Resonance Bank (accession number 16190).

W7 Coordinates and Topology. The computational representation of W7 was defined with the HIC-Up server (http://xray.bmc.uu.se/hicup/) (19) and XPLO2D (ftp://xray.bmc.uu.se/pub/gerard/xutil/) (20) and was manually checked. Xplor-NIH does not incorporate the W7 DIHEdral energy terms from the parameter files, leading to a lack of planarity in the naphthalene moiety of W7. We demonstrated this by obtaining identical results with and without the DIHEdral terms. Consultation with the primary author and maintainer of Xplor-NIH, C. Schwieters (National Institutes of Health, Center for Information Technology), led to the decision to restrain the aromatic ring atom planarity directly with a patch to the IVM module. There is a crystal structure determination of W7 that is consistent with this target geometry (21). The coordinate, topology, and parameter files are included as Supporting Information.

Protein Coordinates and Topology. Initial coordinates were derived from conformer 1 of the cNTnC·Ca^{2+}·Sp·bepridil NMR ensemble (PDB entry 1LXF). Control calculations were also performed using the coordinates from PDB entries 1MXL and 1SPY (cNTnC·Ca^{2+}, reflecting the closed conformation). The protein topology was generated at runtime from its sequence using the Protocol module of Xplor-NIH.

Restrained Docking Protocol. A simulated annealing script, appropriate for NOE-driven docking, was derived from the Xplor-NIH example script, gb1-anneal.py. The script is provided as Supporting Information. All molecular dynamics and energy minimizations were performed with Xplor-NIH's IVM module (22). At each stage in the protocol, the total time can be stipulated and Xplor-NIH varies the step size automatically according to the simulation temperature, the size of the energy gradient, and a parameter approximating the error in the integration of the energies (the ETolerance). In this protocol, short molecular dynamic trajectories are coupled to Powell minimizations having dEPred (the expected energy decrease per step) set to the ETolerance (dEPred = ETolerance).

Dynamics were performed in torsion space except for the initial and final minimization. Three groupings of potential terms

were defined over the simulation. The "base potentials" include all of Xplor-NIH's nonbonded potentials, the intraprotein distance restraints, and the calcium ion restraints. The "docking potentials" included all of the base potentials as well as the protein−W7 distance restraints. The "refinement potentials" included the docking potentials, Xplor-NIH's RAMAchandran (backbone dihedral angle database) potential (23), and the HBDB (dynamic hydrogen bonding) potential (24).

Initial coordinates of W7 and cNTnC·Ca^{2+} were separated by more than 80 Å. Initial velocities were assigned, and the system was equilibrated against the base potentials. During this time, all of the base potential terms were minimized while sampling a small region of conformational space. Next, all protein atoms were immobilized with respect to each other. Any steric (VDW term) interactions between W7 and cNTnC were eliminated. Random velocities were reinitialized, and the system was equilibrated under the docking potentials. Minimization of the docking potentials caused the ligand to dock to a physically impossible location where it would sterically clash with the protein.

The next phase of the calculation reintroduces the steric interactions between protein and W7 atoms. This is done through successive rounds of increasing the scaling of the protein−ligand steric interaction, initializing random velocities, and equilibrating the system (at 25K), and minimization. Forces generated from these interactions do not impact the protein's backbone geometry as backbone atoms are fixed at this time. Instead, the terms of the docking potentials equilibrate over the configuration space of the side chains. Although this stage of the protocol reintroduced the intermolecular steric interaction and consistently minimized the docking potentials, the intermolecular NOE term was never completely satisfied.

In the last stage of the calculation, the velocities from the previous dynamics run were inputted, and the system was equilibrated with all protein atoms reconfiguring against the refinement potentials. During this time, all terms of the docking potential were greatly satisfied: the intermolecular NOE target function usually dropped below 1 kcal/mol (recall, this term is scaled 20-fold to the intraprotein NOE term). Further refinement of this structure followed from consecutive cycles of equilibration for 1 ps and Powell minimization. A final minimization in Cartesian mode was performed and the structure outputted. Ramachandran analysis was performed with Procheck (25). The 10 lowest-energy structures calculated without extra refinement potentials, but with a positive charge on W7's amine nitrogen, are deposited as PDB entry 2KFX.

The Xplor-NIH binary used was downloaded directly from the National Institutes of Health (version 2.21). As the computation time for a structure is dynamically varied over the protocol according to the requested ETolerance and the instantaneous energy gradient, structures determined with this protocol take a varying amount of computational time. A representative calculation of 50 structures took 291 min on a computer with 2 × 2.66 GHz dual-core Intel Xeon processors (using a single core for the calculation), or 5.82 min per structure per core.

RESULTS AND DISCUSSION

Assignment of W7. DMSO was the preferred solvent for the assignment of W7, as this allowed for the preparation of concentrated samples, useful for natural abundance ^{13}C spectroscopy. The ^{1}H and ^{13}C NMR spectra of W7 in DMSO-d_6 (Figures 1 and 2) were difficult to assign. The molecule has two symmetrically arranged aromatic proton spin systems. Only the central spin of each spin system can be identified by direct inspection of the {^{1}H,^{1}H}-DQF-COSY NMR spectrum (Figure 1, left). Craven and others have previously assigned the W7 analogue J8 through the use of analogous compounds lacking the problematically high symmetry (13). Alternate solvents were tested to see if the chemical exchange of the sulfonamide hydrogen could distinguish it from the amine hydrogens, which appears to be the strategy used by Osawa and others (6). W7 was insoluble in methylene chloride, acetone, and chloroform.

Unambiguous assignments were attained through natural abundance ^{13}C spectroscopy at high field (Figure 1). The directly detected ^{13}C spectrum was observed to have a ^{35}Cl/^{37}Cl isotope shift for ring C5, giving rise to two ^{13}C signals with the expected peak separation (1.0 Hz) and relative intensities (26). The key HMBC correlation supporting the unambiguous assignment reflects the magnetization transfer shown by the cyan arrows in Figure 1 at the top left. The expected HMBC correlations are between ring hydrogens and any carbon atoms in a meta relationship (27) (but some weaker ortho couplings are also observed).

The aliphatic tail of W7 (Figure 2) also has a symmetrical ^{1}H spin system, with six methylene groups connecting two nitrogen atoms. The DQF-COSY spectrum allows for unambiguous attribution of the spin system to two ambiguous assignments differing in which terminal methylene is most ring-proximal. This ambiguity can be broken with an additional observation from the titration of cNTnC·Ca^{2+} into W7, where the downfield resonance (∼2.8 ppm) undergoes line broadening concomitant with similar broadening in the aromatic ring atoms (see Figure 3). Since position 11 is more proximal to the aromatic ring, we assign it to the signal at 2.8 ppm.

Binding of cNTnC·Ca^{2+} to W7. The titration of cNTnC into a W7 sample made up in aqueous buffer is shown in Figure Supp-3 of the Supporting Information (described in Materials and Methods as titration 1). This titration is the reverse of the usual titration of the ligand into the protein sample and, therefore, can more directly disclose the binding at high protein:ligand ratios. This experiment was replicated with more strongly controlled pH (Figure 3). These spectra are in the NMR fast exchange limit for the chemical exchange between the free and bound forms, so the W7 resonances (shown for the free ligand in the bottom trace; the assignments of W7 in H$_2$O can be directly transferred from DMSO since the spectra are very similar) can be tracked through the titration to their final positions as the protein:ligand ratio approaches 1:1. Chemical shifts of W7 in the bound state can be compared with those assigned for W7 when complexed with calmodulin. As W7 is titrated into the cNTnC·Ca^{2+} system, H4 and H8 exchange their order on the frequency coordinate; this is not observed as W7 is titrated into the Ca^{2+}-saturated CaM system (6).

The most-downfield W7 signal changes the most upon cNTnC·Ca^{2+} binding and was selected for analysis. The peak frequencies were extracted from the 1D spectra in VnmrJ, and the titration curve is plotted in Figure 4. These data cannot be fit to a single-site binding model as in previous work (9). Also, these data cannot be fit to a two-site, sequential model. As such, the appropriate form of a binding model describing this equilibrium would allow stoichiometries higher than 1:1 binding. The
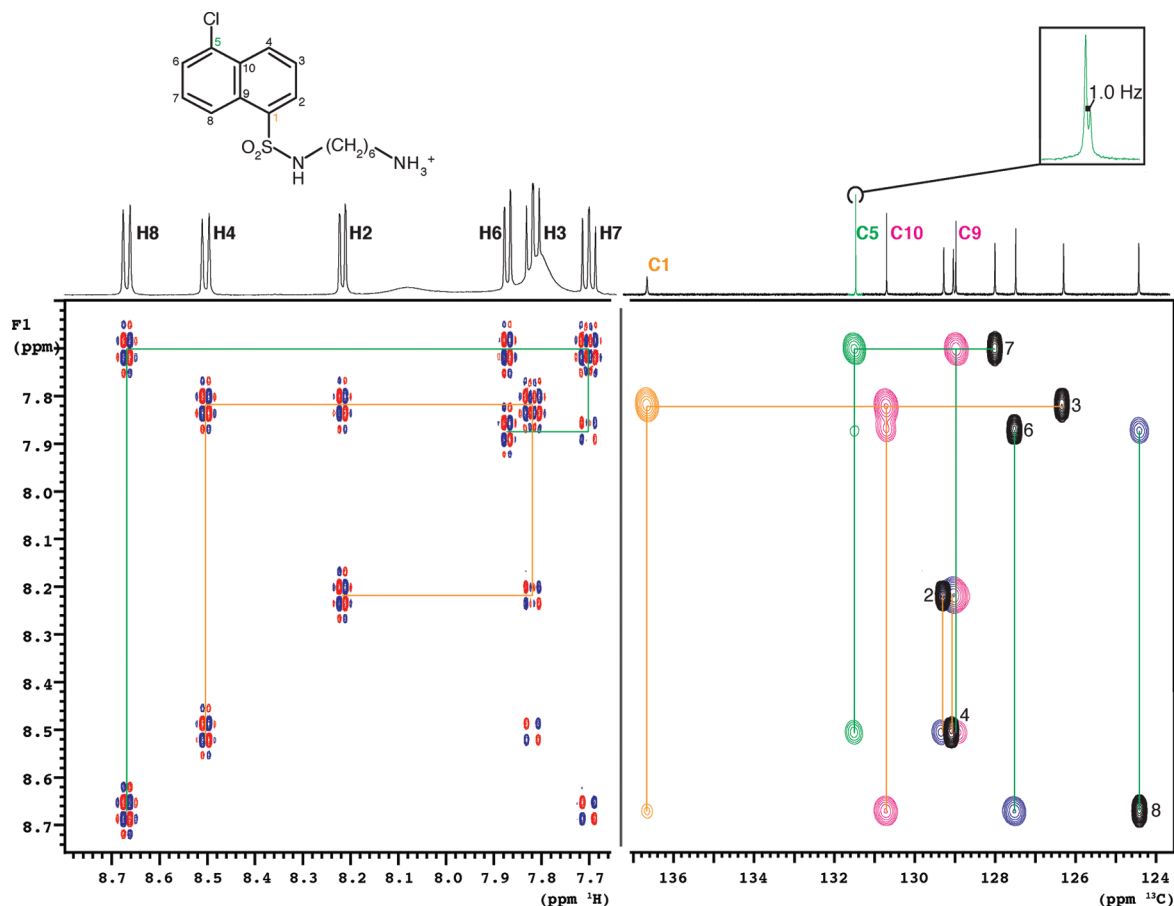
FIGURE 1: Assignment of the aromatic system in W7. The protons form two spin systems, with only the central spins (protons 3 and 7) forming an ambiguous pair. The two spin systems are shown with green or orange correlations in the {¹H,¹H}-DQF-COSY spectrum [two-dimensional (2D) spectrum at left]. We resolve this ambiguity with a high-resolution ¹³C one-dimensional spectrum (top right), which shows a single 1 Hz splitting because of the ³⁵Cl/³⁷C ¹³C isotope shift; this observation unambiguously identifies C5. The {¹H,¹³C}-HMBC spectrum (2D spectrum at right, with colored peaks) shows the expected two-bond correlation between H7 and C5. This also disambiguates H3 by exclusion. These assignments are further corroborated by the absence of {¹H,¹³C}-HSQC peaks (2D spectrum at right, black peaks with labels corresponding to proton–carbon pairs) at the ¹³C frequencies for C5 and C9. The other HMBC signals correlating to C5 and C9 arise from H4. With the proton and carbon assignments for positions 3 and 4, position 2 is known by exclusion. Position 8 is identified from its HMBC correlations to C1 and C10, leaving position 6 assignable by exclusion.

following equilibrium was proposed:

$$P + L \leftrightarrow P \cdot L \leftrightarrow P \cdot L \cdot L_n \qquad (1)$$

where P is the protein (cNTnC·Ca²⁺) and L is the ligand (W7). The model has two equilibrium constants, K_{d1} and K_{d2}, equal to [P][L]/[PL] and [P·L][L]^n/[P·L·L$_n$], respectively. The binding constant for the second step, as well as the stoichiometry of the second binding event (n), allows for modeling of secondary nonspecific binding. One mole of P·L·L$_n$ reflects the binding of $n + 1$ ligand signals. Although the model, as written, implies a simultaneous binding of n molecules of ligand, we chose it to absorb the combined uncertainties of choosing a single K_{d2} to summarize the process and modeling the spectral perturbation of all ligands as equal in magnitude. So K_{d2} and n are covariant parameters.

This model cannot be solved analytically, but numerical simulation (see Figure 4) allows for confirmation that the form of the model is appropriate. The following parameter values were used: $K_{d1} = 100$ μM, $K_{d2} = 0.43$ pM, and $n = 4$. The secondary binding then has a microscopic binding constant of 0.43 pM$^{1/4}$ ~ 0.8 mM. Equation 1, with the parameters described above, predicts that at the 1:1 point, the P·L complex populates 83.4% of the protein species, with only ~0.5% of the protein

species in the nonspecific P·L·L$_n$ complex (the remainder being free protein). Therefore, appropriate conditions for structure determination are obtained close to a 1:1 protein:ligand ratio.

Of course, the proposed equilibrium differs in mechanism from the single-site fits reported by ourselves (9) and Hidaka and others (11). As NMR has limited sensitivity, strong binding events and nonunitary stoichiometries are not always identified. However, this is offset in part by its tremendous site-specific resolution. For example, the amide-detected binding in reference 9 could be fit to a single-site binding model, but the Met Cε signals reported in that study disclose more complicated binding phenomena. Similarly, Hidaka and others report a single K_d for the sTnC·4Ca²⁺–W7 equilibrium, although their Scatchard plot demonstrates pronounced nonlinearity.

Conformational Dynamics of W7. The T_1 relaxation times of protons are dominated by the dipolar relaxation mechanism (28). The aromatic protons of unbound W7 show two classes of relaxation times (Table 1). The contribution of a vicinal proton to dipolar relaxation accounts for the substantially shorter T_1 values for protons at positions 3 and 7 compared with the other ring protons. The expression

$$1/T_1 \propto N(\gamma^4\hbar^2/r_{HH}^6)\tau$$

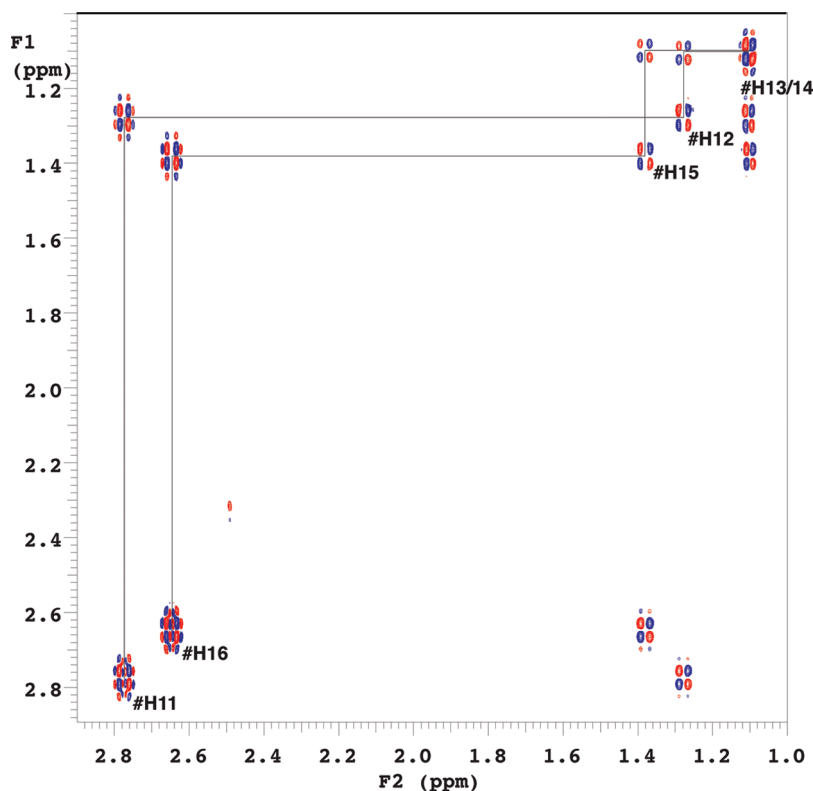FIGURE 2: {^{1}H,^{1}H}-DQF-COSY NMR subspectrum of the aliphatic tail of W7. Although the spin system can be unambiguously attributed, assignment of the terminal positions (*11*, *16*) requires additional data. Considering that the line width of the more downfield signal line broadens in response to cNTnC·Ca^{2+} binding concurrent with the broadening in the aromatic ring (Figure 3), we take that signal to be the more ring-proximal signal (position 11).
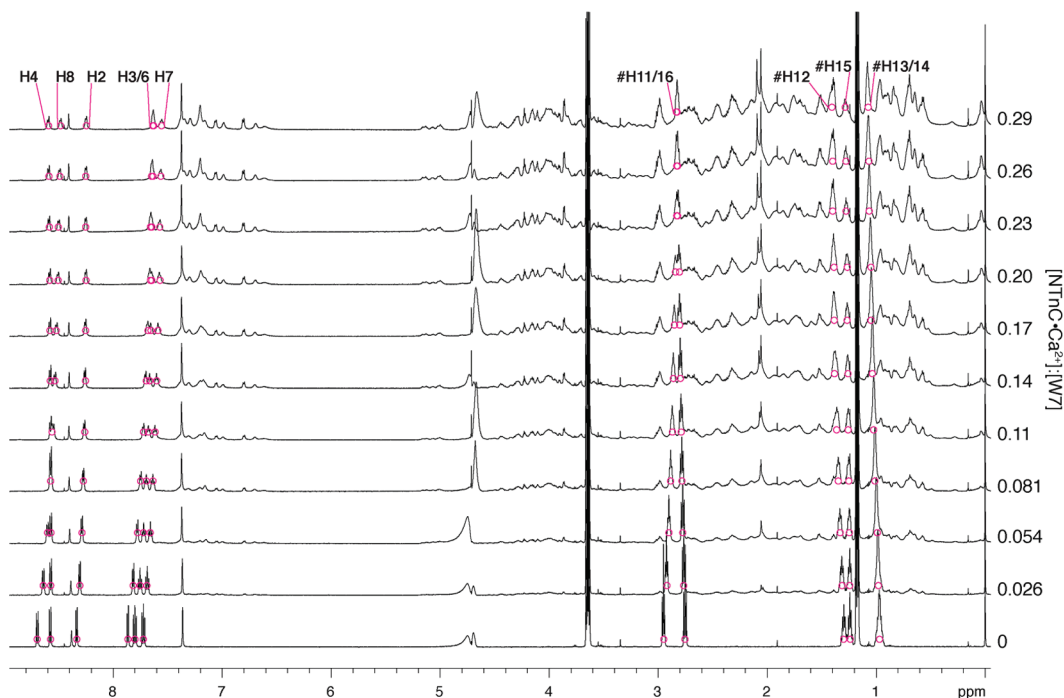

FIGURE 3: Binding of cNTnC·Ca^{2+} to W7, monitored with 1D ^{1}H spectra. A buffered stock solution of cNTnC·Ca^{2+} was used, affording more control over the pH changes over the titration. The protein:W7 ratio is shown to the right of each spectrum. cNTnC·Ca^{2+} binding induces chemical shift changes. The binding curve rises more steeply than would be observed for 1:1 binding. The equilibrium can be modeled in terms of a microscopic affinity similar in magnitude, however (Figure 4). Assignments for W7 in the unbound state (Figures 1 and 2) were transferred to those of the bound state through these spectra.

describes ^{1}H T_1 relaxation times for a dipolar mechanism in the extreme narrowing limit ($\tau\omega \ll 1$), where τ is the rotational correlation time for a W7 proton, ω is the spectrometer

frequency, and N is the number of proton neighbors. In this limit, T_1 is inversely correlated with the correlation time. The value of r_{HH} is much shorter for the tail protons than the
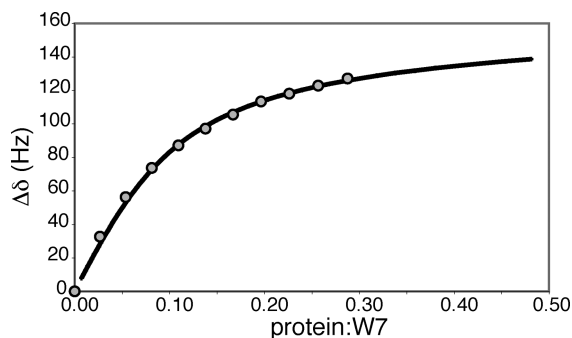
FIGURE 4: Simulation of cNTnC·Ca^{2+}−W7 binding equilibria. The downfield W7 signal (H8) from titration 2 (Figure 3) can be fit to an $n + 1$ site, sequential binding model, where n is the number of secondary (nonspecific) binding sites. The circles are the data points, and the closely spaced plus signs reflect the numerical simulation. The parameter values used are as follows: $K_{d1} = 100\ \mu M$, $K_{d2} = 0.43\ pM$, and $n = 4$.

aromatic protons, so the T_1 values are expected to be shorter for the tail protons. The mobility of the qth tail atoms can be approximated, relative to those in position 11.

$$\tau_q/\tau_{11} \approx T_{1,11}/T_{1,q}$$

Table 2 lists the incremental mobilities for the W7 tail atoms calculated from the measured relaxation times using the above relationship. Protein binding serves to globally shorten the T_1 values and make them more uniform. This may reflect changes in mobility (indicating that the tail of W7 is less mobile when bound), contributions to relaxation from additional proton neighbors, and spin diffusion when it is bound to the protein. Detailed interpretation of these data is limited from ambiguities in the binding equilibrium; as modeled above, the sample at this point (18% protein:W7 molar ratio) contains almost equal quantities of the 1:1 complex and the higher-order, nonspecific complexes.

NMR Structures. The structure calculation consisted of the simulation of 50 conformers with different random seeds for all velocity initializations. Two variables were permuted, giving four NMR ensembles. One variable was the introduction of a positive charge into the amine nitrogen of W7. Ensembles with this manipulation have names appended with a Q. The other variable was the incorporation of Xplor-NIH's refinement potentials, as described in Materials and Methods. Ensembles with this manipulation are named "refined" as opposed to "plain". Table 3 summarizes some of the properties of the four ensembles. All ensembles extensively minimize the target (docking) potential. In terms of convergence of the solution and maximal satisfaction of the docking potential, the "plainQ" calculation was most attractive and was selected for further analysis.

The 50 structures vary in the residual energy in the docking term, from 0.017 to 0.175 kcal/mol; 46 of the 50 calculated structures had no violations in the docking term (the other four structures had a single violation.) As shown in Figure 6, the entire ensemble positions W7 similarly, with the only remaining point of convergence being the details of the pose. Considering the 10 best solutions (lowest energies overall), a single pose is favored with a defined conformation for W7's tail (Figure 7). None of these structures have violations in the docking term, although they do have other inadequacies.

Many of these limitations (including stereochemical quality) reflect sources of imprecision external to the docking term: a

Table 2: Correlation Times of Tail Atoms Expressed as a Fraction of the Correlation Time of the Most Ring-Proximal Tail Protons (site 11)

signal	τ_q/τ_{11}	
	free W7	18% (molar ratio) cNTnC·Ca^{2+}:W7
H11	1.0	1.0
H12	0.90	1.22[a]
H13/14	0.87	1.05
H15	0.66	1.22[a]
H16	0.52	1.22

[a] T_1 values correspond to more than one signal due to spectral overlap.

control calculation sharing the plainQ simulation parameters but lacking the docking potential gave similar energies and Ramachandran statistics. WHAT-CHECK (*29*) runs on the initial coordinates (PDB entry 1LXF), the coordinates determined with our intraprotein restraints (PDB entry 1MXL), and structures calculated in this study (PDB entry 2KFX) all gave poor scores in a number of metrics, especially intramolecular contacts or "bumps". These close contacts for 2KFX were not corroborated by the (ADIT) upload servers for the PDB or BMRB. The inclusion of solvent may improve the agreement with target metrics (*30*); however, this study blends prior and posterior information in a way that presupposes some amount of disagreement between an accurate structure and the intraprotein restraints. Further refinement of the solution in the presence of violated restraints is likely an exercise in over-refinement.

In contrast to the intermolecular distance restraints, the intraprotein restraints used to define the open conformation of cNTnC·Ca^{2+} (*3*), though well-validated by a subsequently determined crystal structure (*31*), are only approximately valid when applied toward a cNTnC·Ca^{2+}·W7 complex. They can be considered control restraints. As such, should ligand binding deform the protein conformation beyond the previously determined conformation, the control restraints will report the discrepancy by increasing the system's energy. Should ligand binding prove to be completely compatible with the intraprotein NOEs, this would further illustrate how the information content of the intraprotein NOEs may not unambiguously define a conformation, although a single-conformer interpretation of the NOE tends to give highly converged structures (*32*).

All structures had some violations in the intraprotein NOE term; the 10 best solutions have residual NOE energies in the range of 3.9−5.3 kcal/mol, amounting to four to six violations. There were 17 different violated intraprotein restraints, with seven restraints being violated in the majority of structures. Of these, four were long-range restraints. One restraint, colocalizing atoms from Met80 and Phe27 to 3.85 Å, is violated (calculated distance of ~7 Å) because Met80 instead stabilizes W7 in the complex. Two other violated restraints colocalize Phe27 and Leu41 (target distance of 3.56 Å) and colocalize V28 and Ser35 (target distance of 3.07 Å), with calculated distances of ~6 Å. These restraints are close to the (defunct) site 1, which may vary from the coordinates of 1MXL, especially since this region undergoes conformational exchange in solution (*33*). Also, a restraint between the HN group of Glu66 and Hγ1 of Glu76 was usually violated (target distance of 2.98 Å; calculated distance of ~5 Å). This violation may reflect a competition (frustration) between the intraprotein and Ca^{2+}-coordinating potentials.

As the docking is effected through 31 distance restraints, these data could be exhaustively cross-validated (Figure 6B).

Table 3: Ensemble Energies and Statistics (best 10 of 50 structures)

ensemble	total energy (kcal/mol)	docking energy (kcal/mol)	Ramachandran plot occupancy (%)			
			favored	additional	generous	disallowed
plain (ae7b1)	99−106	0.021−0.068	71.8	25.8	2.3	0.1
plainQ (ae7b4)	99−102	0.017−0.057	71.1	26.2	2.7	0.0
refined (ae7b2)	−910 to −821	0.068−0.155	85.1	14.3	0.6	0.0
refined (ae7b3)	−858 to −825	0.050−0.127	85.3	14.1	0.6	0.0
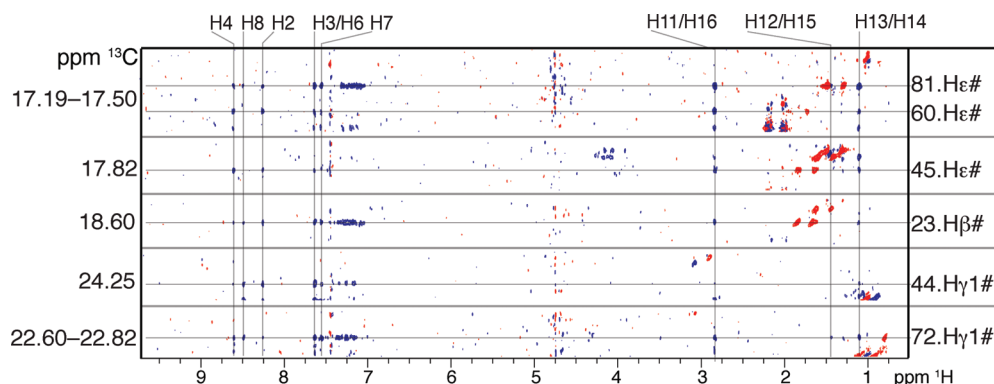
FIGURE 5: Intermolecular NOEs between W7 and cNTnC·Ca^{2+}. The NOEs were observed through a $\{^{13}C,^{1}H\}$-edited, $\{^{12}C,^{1}H\}$-filtered NOESY experiment. Signals with positive amplitude (signals, noise, or artifacts) are shown as blue contours, and negative signals (noise or artifacts) are shown as red contours. Assigned strips for a given ^{13}C range are shown as separate panels along with markers indicating the assigned protein ^{1}H signal. A number of "bleed-through" signals that originate from the protein but survive the ^{12}C filter occur in the aromatic region of the spectrum. To assign these data in the presence of the artifacts, peaks at the ligand frequencies were exclusively considered (labels at top).
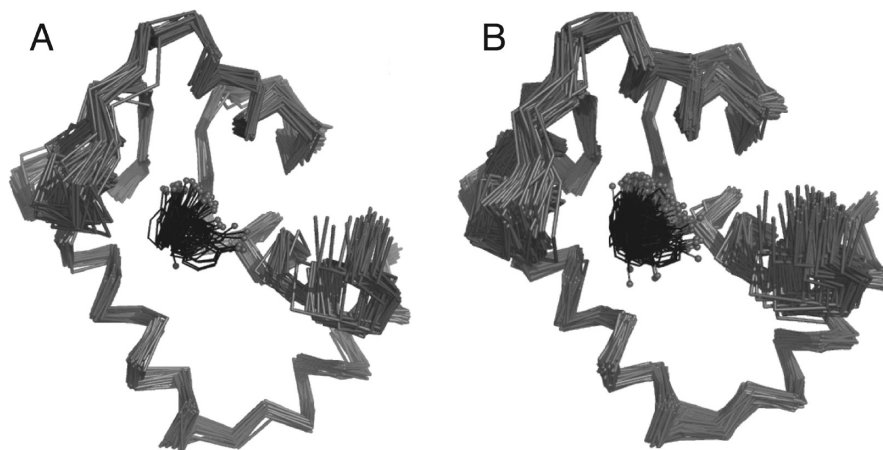

FIGURE 6: All structures calculated in the fully determined and cross-validation trials for the plainQ calculation. The protein backbone is depicted with a Cα trace (one vertex per Cα) with W7's non-hydrogen atoms shown as sticks. The aromatic atoms of W7 are colored black with the chlorine atom depicted as a gray sphere. (A) Complete set of docked structures for ensemble plainQ. The solutions all cluster to the same binding site; however, additional discrimination (exclusion of higher-energy structures) is required to visualize the most-probable pose. The lowest-energy structures from this ensemble are presented in Figure 7. (B) Complete set of docking cross-validation trials for ensemble plainQ. Depictions are as in panel A. Eliminating single restraints from the docking solution does decrease the convergence of the ligand pose; however, the localization of the binding site is impervious to these perturbations.

Thirty-one replica calculations were performed (10 structures per run), each with one restraint inactivated. All cross-validation trials allowed for good minimization of the intermolecular NOE term. Some conformers place the orientation of the ring in an alternate pose; however, no alternate solution was stabilized consistently over the cross-validation trial. To assess convergence, the results of these runs are compared with all 50 structures of the plainQ ensemble in Figure 6A (not just the low-energy structures).

Examining both the fully determined and cross-validated ensembles shows the different atoms of W7 varying in convergence to differing extents. The two alternative poses pivot the chloronaphthalene group around C1 (the sulfonamide-coupling carbon of W7). As such, the level of convergence for some ligand atoms is quite high, because even low-quality docking solutions leave the positions unchanged for those atoms. The precision of the W7 coordinates was quantified by calculating the mean square deviation from the lowest-energy cross-validation trial (after alignment of the protein backbone atoms). To report an estimate of the precision of the ensemble, the root-mean-square deviation (rmsd) of each atom in W7 was calculated on the basis of the entire cross-validated trial. Via calculation of these
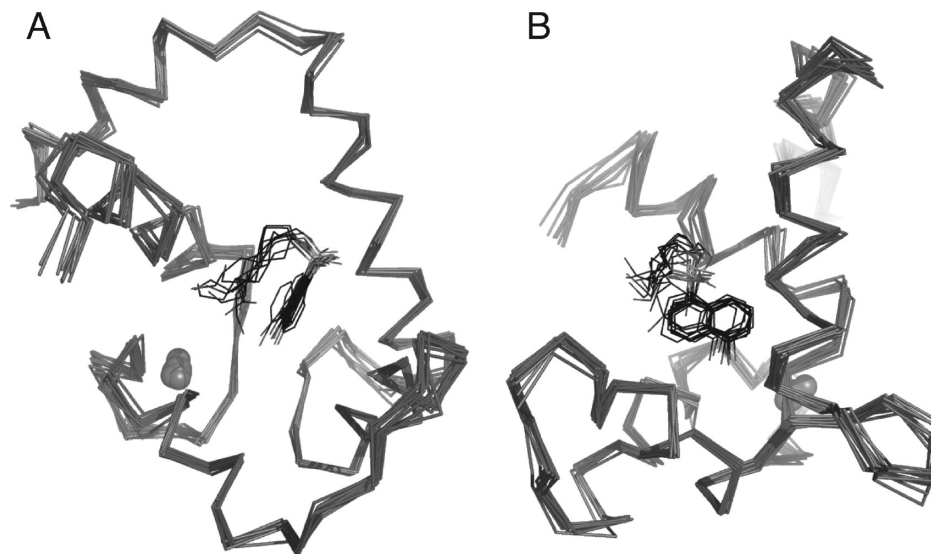
A

B

FIGURE 7: Ten lowest-energy conformers (best 20%) from the plainQ calculation. Depictions are as in Figure 6, but the Ca^{2+} ions are also shown, as gray spheres. The non-carbon atoms of W7 are colored gray; hydrogens are not shown. (A) The N-terminal helix (helix N) of cNTnC is at the top of the figure pointing to the left and down. Helix D is pointing out of the page. (B) A different orientation of the same ensemble. Helices A and B are closest to the reader.

precisions from the cross-validated trials, the potential influence of errors in the intermolecular NOEs is also considered. The atom-specific rmsds for W7's non-hydrogen atoms are listed in Table 4. The atoms surrounding C1 are the most precisely determined (1−3 Å rmsd), and the tail atoms are the least defined (3−6 Å rmsd). It is also useful to estimate the precision of the protein coordinates. Procheck can assign "equivalent resolutions" based on an ensemble's conformity to target covalent parameters. On the basis of the Ramachandran statistics of the ensemble [the poorest-performing metric assessed by Procheck (*25*)], the equivalent resolution is 2.8 Å.

Structure Determination Protocol. Our procedure for "crystal soaks by NMR" gradually introduces the protein−ligand steric interaction after initial satisfaction of the docking potential. As such, the conformational search is biased toward a maximally complementary fit following satisfaction of the docking restraints. An implication of this is that the maximal conformational search size is a function of the ligand volume, but the protocol uses a large amount of prior information besides ligand volume.

The agreement of the prior data with the new experimental data can be assessed by noting the residual in the docking potential following the initial (no-intermolecular-sterics) docking. At this point of the simulation, the intermolecular potential has had no opportunity to influence the protein coordinates, so this term is therefore an independent measure of the agreement between the prior and posterior data. The ability of this residual to discriminate between good and poor agreements is now illustrated through examples with inappropriate choices of prior information. We know that W7 binding stabilizes the open conformation of $cNTnC \cdot Ca^{2+}$ (*9, 10*) so the most inappropriate intraprotein NOEs for the docked complex would reflect the closed conformation of PDB entry 1SPY (*2*). The choice of the initial coordinates and intraprotein NOEs of 1SPY gives an intraprotein NOE residual of 3.25 ± 0.65 kcal/mol (mean ± standard deviation over all 50 conformers) but does not minimize the docking residual (314 ± 38 kcal/mol). For the choice of an inappropriate combination of initial coordinates and intraprotein NOEs (the initial coordinates from 1SPY with the

Table 4: Root-Mean-Square Deviations for the Non-Hydrogen Atoms of W7 in the Cross-Validation Trials

atom	rmsd (Å)	atom	rmsd (Å)
C1	1.077	O2	2.365
C9	1.162	N1	2.944
C2	1.352	O1	3.054
C8	1.367	CL1	3.272
S1	1.666	C11	3.974
C10	1.762	C14	4.429
C7	1.763	C13	4.504
C3	1.909	C12	4.510
C6	2.165	C16	5.061
C4	2.169	C15	5.289
C5	2.269	N2	6.191

intraprotein NOEs of 1MXL), the intraprotein NOE residual is 58 ± 12 kcal/mol and the docking residual is 369 ± 76 kcal/mol. In contrast, the use of appropriate initial coordinates and intraprotein NOEs (as in the plainQ calculation) gives a small residual for the intraprotein NOEs (7.22 ± 3.69 kcal/mol) and good satisfaction of the docking potential (17.07 ± 6.96 kcal/mol). The initial docking residuals thus provide a strong criterion for the selection of prior data.

The issues surrounding the mutual weighting of known and assumed information are endemic to structure determination by NMR, as no NMR structure is actually overdetermined. A useful approach to this problem is outlined by Nilges and co-workers (*34, 35*), who stress that structure determination is an example of data inversion and that the weightings of NOE-derived distance restraints are parameters that should be marginalized. In this study, we do not apply the inferential structure determination protocol, although our approach could be harmonized with it. An immediately presenting (but nonconfounding) complication is that inferential structure determination as originally developed (*34*) treats the (all of the) NOE data as posterior knowledge and the target covalent parameters as prior knowledge. Here, the Ca^{2+} binding restraints are not derived from NOE data at all and in general will not have similar weightings to the correctly weighted potential for inverting the NOE data into
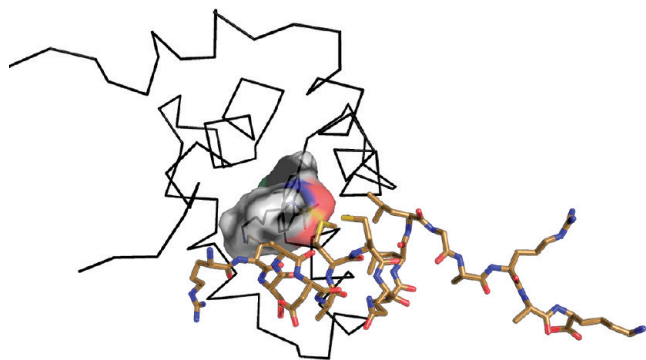
FIGURE 8: Comparison of the lowest-energy conformer of the cNTnC·Ca^{2+}·W7 complex with the first conformer of cNTnC·Ca^{2+}·Sp (PDB entry 1MXL). The structures were aligned over the backbone heavy atoms of residues 2−87 (2.46 Å rmsd). The backbone of cNTnC·Ca^{2+} from 1MXL is shown as a black Cα trace. The switch peptide (cardiac TnI$_{147-163}$) is shown as sticks, with carbon atoms colored light brown. W7 is shown with black sticks for carbon atoms and with the surface represented as a transparent outline. This shows that W7 serically interferes with the stabilizing cNTnC−Sp interactions originating from Ile149 and Met154. The terminal amine group of W7 may compete with Arg148 for electrostatic interactions with acidic patches on helices C and D.

distance restraints. Also, marginalizing over all possible weightings does not reflect our knowledge of the causal priority of Ca^{2+} binding to W7 binding, and the high accuracies and precisions provided by good crystal structures.

A basic limitation to our calculations is that the energy gap between maximally converged and unconverged ligand poses is small. Distinction should be made between assessment of convergence (or precision) and maximal satisfaction of the target function (which reflects accuracy). As the both the refined and the refinedQ calculations have higher final values of the docking potential than either of the plain calculations, the solution is less accurate. Xplor-NIH's refinement potentials (the RAMA and HBDB potentials) are not intended to greatly perturb convergence of the solution. In this study, the introduction of these two terms perturbed the convergence of the amine tail conformation (together, and with the weightings inherited from the gb1-anneal.py example script). This may reflect the need for the most pertinent data (the docking potential) to dominate the simulation energetics. Perhaps more judicious weighting of the two terms or exclusion of one of them would improve the backbone stereochemistry of the model without compromising convergence.

Mechanistic Implications. Ca^{2+} binding to skeletal NTnC (2 molar equiv of Ca^{2+}) induces a conformational change that allows it to bind to the switch region of skeletal troponin I (*36*). This conformational transition results in the solvent exposure of a hydrophobic surface and is energetically unfavorable under ambient conditions. This conformational transition (dubbed "opening") has been explained in terms of a cascade originating with the reorientation of the side chains in the Ca^{2+}-binding sites and propagating across the tertiary structure (*37, 38*). A point mutation of skeletal NTnC (E41A) abolishes the Ca^{2+}-induced conformational change (but not Ca^{2+} binding), which shows that opening is effected through a mechanistic cascade, specifically mediated through the N-terminal Ca^{2+}-binding site (site I) (*38*). In the cardiac system, Ca^{2+} binding to site I is defunct, and the structure is not observed to open following the binding of 1 equiv of Ca^{2+}. Addition of Sp, however, stabilizes the open conformation.

FIGURE 9: Comparison of the cNTnC·Ca^{2+}·W7 structure with the cNTnC·Ca^{2+}·Sp·bepridil structure (PDB entry 1LXF). The lowest-energy conformer from the plainQ calculation (black and gray carbon atoms) is aligned to the first conformer of 1LXF (light brown carbon atoms, backbone rmsd of 1.50 Å). The Sp component of 1LXF is not shown. W7's binding site only partially overlaps with bepridil's. The primary amine of W7 colocalizes to one of bepridil's tertiary amines. W7 penetrates more deeply into the hydrophobic pocket of cNTnC·Ca^{2+} than bepridil when bound to cNTnC·Ca^{2+}·Sp.

When binding is accompanied by conformational changes in the protein, the change in conformation can precede or follow from the binding. The former mechanism is called "conformational selection" and the latter "induced fit". Both mechanisms have been advanced throughout the literature in a plethora of contexts, including the association of cNTnC·Ca^{2+} with Sp. In the induced fit model, Ca^{2+} binding to the cardiac system "sets the stage" for Sp binding, helping to overcome the "energetic barrier to opening". The existence of a substantial energy barrier seems unlikely, given results indicating that cNTnC·Ca^{2+} undergoes conformational exchange attributable to opening (*33, 39, 40*). Further support for the conformational selection mechanism for the association of cNTnC·Ca^{2+} with Sp comes from the fact that W7 and Sp both stabilize the open conformation of cNTnC·Ca^{2+} (*9, 10*). As W7 is a poor structural analogue of Sp (being aromatic, much smaller, and less functionalized), it seems improbable that it is capable of mimicking an induced fit process. A more parsimonious explanation is that the target peptide and W7 both bind to and stabilize a preexisting open conformation as in the conformational selection mechanism.

Structure−Activity Relationships. Previous work has motivated and supported a "switch-peptide-occlusion" mechanism for W7's inhibition of striated muscle contraction (*7, 9, 10*). This means that W7 binds to cNTnC·Ca^{2+} and impedes the subsequent binding of Sp. These results substantiate such a mechanism because the overall binding site of W7 is unambiguously localized to the previously proposed Sp binding site (see Figure 8). As shown in Figure 9, the W7 binding site is similar but not identical
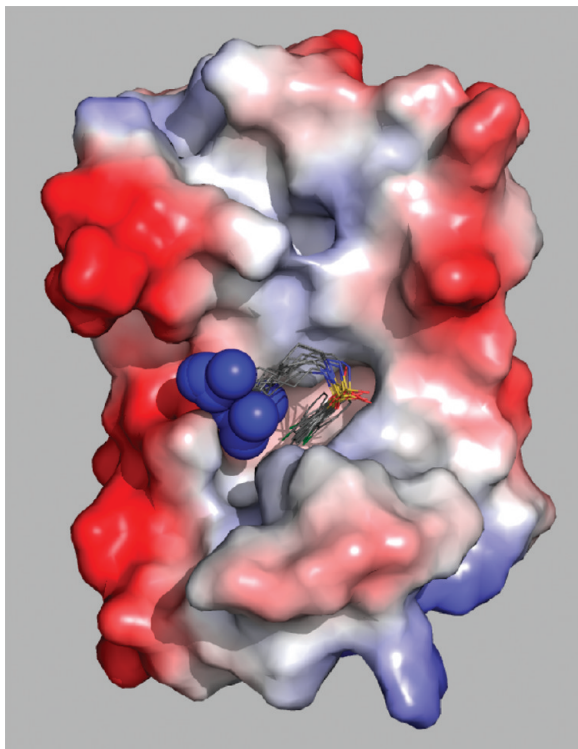
FIGURE 10: Vacuum electrostatics of the cNTnC·Ca^{2+}·W7 complex. The surface of the lowest-energy conformer from the plainQ calculation is depicted with an electrostatic potential map so that regions of negative charge are colored red and positive charge blue; heteroatoms are colored as in Figure 7. The terminal amine of W7 is depicted with a sphere to approximate this moiety's positive electric field. Besides sterically occluding the binding of the switch peptide, W7 may attract helices C and D to each other (stabilizing the inactive, closed conformation) or destabilize interactions between helix D and the inhibitory region in the active state.

to the location of bepridil when bound to cNTnC·Ca^{2+}·Sp. Both bepridil and W7 bind to cNTnC·Ca^{2+}·Sp with weaker affinity than to cNTnC·Ca^{2+} (*4*, *10*); however, Sp binding does not preclude W7 binding (*10*), so one could assume that Sp, when bound, shifts the binding site for W7 to one more analogous to bepridil in the cNTnC·Ca^{2+}·Sp·bepridil complex (*4*).

To date, structure−activity relationships of W7 have been defined almost exclusively in terms of its hydrophobicity. The chloronaphthalene moiety is the best-rationalized, as most explicitly disclosed by the structure of its CaM-bound state (*6*). Substitution of the chlorine atom with more polarizable halogens enhances both CaM affinity and biochemical activity (*41*), indicating that the bound state is hydrophobically stabilized. Increasing the tail length of W7 increases its affinity and the activity in the CaM system but also its hydrophobicity. The structures of neither CaM·4Ca^{2+}·W7 nor CaM·4Ca^{2+}·J8 show ordering in the tail moiety. The T_1 analysis (Table 2) indicates that in the cTnC·Ca^{2+}·W7 complex the tail moiety does order in the complex, consistent with the structure determination.

As shown in Figure 10, the conformation of W7's tail in the bound state places the terminal amine moiety in the proximity of two acidic patches located on helices C and D. This electrostatic interaction facilitates maximal satisfaction of the docking potential (Table 3). By drawing helices C and D closer to each other, W7 may interfere with the stabilization of the inhibitory region of TnI, which binds to helices D and E of TnC (*31*). The W7 amine

group may compete with the guanidino moiety of Arg148 of Sp, which also interacts with the aforementioned acidic patches (Figure 8). This novel structure−activity relationship for the amine tail moiety suggests that W7 is bidentate and further implicates the importance of electrostatic interactions in the structure−function relationship of troponin C (*42*).

SUPPORTING INFORMATION AVAILABLE

Representative fitted T_1 relaxation curves from the titration of W7 with cNTnC·Ca^{2+} (Figure Supp-1), assigned signals of the {^{1}H,^{13}C}-HSQC spectrum (Figure Supp-2), a replica titration monitored by proton NMR (called titration 1 in Materials and Methods) (Figure Supp-3), topology, parameter, and coordinate files for W7, and the script used for the structure determination with Xplor-NIH. This material is available free of charge via the Internet at http://pubs.acs.org.

REFERENCES

1. Dominguez, C., Boelens, R., and Bonvin, A. M. J. J. (2003) HAD-DOCK: A protein-protein docking approach based on biochemical or biophysical information. *J. Am. Chem. Soc. 125*, 1731–1737.
2. Spyracopoulos, L., Li, M. X., Sia, S. K., Gagne, S. M., Chandra, M., Solaro, R. J., and Sykes, B. D. (1997) Calcium-induced structural transition in the regulatory domain of human cardiac troponin C. *Biochemistry 36*, 12138–12146.
3. Li, M. X., Spyracopoulos, L., and Sykes, B. D. (1999) Binding of cardiac troponin-I147−163 induces a structural opening in human cardiac troponin-C. *Biochemistry 38*, 8289–8298.
4. Wang, X., Li, M. X., and Sykes, B. D. (2002) Structure of the regulatory N-domain of human cardiac troponin C in complex with human cardiac troponin I147−163 and bepridil. *J. Biol. Chem. 277*, 31124–31133.
5. Zhang, M., Tanaka, T., and Ikura, M. (1995) Calcium-induced conformational transition revealed by the solution structure of apo calmodulin. *Nat. Struct. Biol. 2*, 758–767.
6. Osawa, M., Swindells, M. B., Tanikawa, J., Tanaka, T., Mase, T., Furuya, T., and Ikura, M. (1998) Solution structure of calmodulin-W-7 complex: The basis of diversity in molecular recognition. *J. Mol. Biol. 276*, 165–176.
7. Adhikari, B. B., and Wang, K. (2004) Interplay of troponin- and myosin-based pathways of calcium activation in skeletal and cardiac muscle: The use of W7 as an inhibitor of thin filament activation. *Biophys. J. 86*, 359–370.
8. Li, M. X., Robertson, I. M., and Sykes, B. D. (2008) Interaction of cardiac troponin with cardiotonic drugs: A structural perspective. *Biochem. Biophys. Res. Commun. 369* (1), 88–99.

9. Hoffman, R. M. B., Li, M. X., and Sykes, B. D. (2005) The binding of W7, an inhibitor of striated muscle contraction, to cardiac troponin C. *Biochemistry 44*, 15750–15759.

10. Li, M. X., Hoffman, R. M. B., and Sykes, B. D. (2006) Interaction of cardiac troponin C with W7 in the presence of three functional regions of cardiac troponin I. *Biochemistry 45*, 9833–9840.

11. Hidaka, H., Yamaki, T., Naka, M., Tanaka, T., Hayashi, H., and Kobayashi, R. (1980) Calcium-regulated modulator protein interacting agents inhibit smooth muscle calcium-stimulated protein kinase and ATPase. *Mol. Pharmacol. 17*, 66–72.

12. Hoffman, R. M. B., Li, M. X., and Sykes, B. D. (2005) Structural bases for the activity of W7, an inhibitor of striated muscle contraction. Presented at Keystone Symposia: Frontiers of NMR in Molecular Biology IX, Banff, AB, Jan. 29–Feb. 4, 2005.

13. Craven, C. J., Whitehead, B., Jones, S. K., Thulin, E., Blackburn, G. M., and Waltho, J. P. (1996) Complexes formed between calmodulin and the antagonists J-8 and TFP in solution. *Biochemistry 35*, 10287–10299.

14. Chandra, M., Dong, W. J., Pan, B. S., Cheung, H. C., and Solaro, R. J. (1997) Effects of protein kinase A phosphorylation on signaling between cardiac troponin I and the N-terminal domain of cardiac troponin C. *Biochemistry 36*, 13305–13311.

15. Baryshnikova, O. K., Williams, T. C., and Sykes, B. D. (2008) Internal pH indicators for biomolecular NMR. *J. Biomol. NMR 41*, 5–7.

16. Delaglio, F., Grzesiek, S., Vuister, G. W., Zhu, G., Pfeifer, J., and Bax, A. (1995) NMRPipe: A multidimensional spectral processing system based on UNIX pipes. *J. Biomol. NMR 6*, 277–293.

17. Johnson, B. A. (2004) Using NMRView to visualize and analyze the NMR spectra of macromolecules. *Methods Mol. Biol. 278*, 313–352.

18. Lee, W., Revington, M. J., Arrowsmith, C., and Kay, L. E. (1994) A pulsed field gradient isotope-filtered 3D ^{13}C HMQC-NOESY experiment for extracting intermolecular NOE contacts in molecular complexes. *FEBS Lett. 350*, 87–90.

19. Kleywegt, G., and Jones, T. (1998) Databases in protein crystallography. *Acta Crystallogr. D54*, 1119–1131.

20. Kleywegt, G. (1995) Dictionaries for Heteros. *CP4/ESF-EACBM Newsletter on Protein Crystallography 31*, 45–50.

21. Hempel, A., Camerman, N., Mastropaolo, D., and Camerman, A. (2005) Calmodulin antagonists: Structure of N-(6-aminohexyl)-5-chloro-1-naphthalenesulfonamide hydrochloride (W-7) and comparison with trifluoperazine (TFP)–Calmodulin binding. *Can. J. Chem. 83*, 1141–1145.

22. Schwieters, C. D., and Clore, G. M. (2001) Internal coordinates for molecular dynamics and minimization in structure determination and refinement. *J. Magn. Reson. 2*, 288–302.

23. Kuszewski, J., Gronenborn, A. M., and Clore, G. M. (1996) Improving the quality of NMR and crystallographic protein structures by means of a conformational database potential derived from structure databases. *Protein Sci. 5*, 1067–1080.

24. Grishaev, A., and Bax, A. (2004) An empirical backbone-backbone hydrogen-bonding potential in proteins and its applications to NMR structure refinement and validation. *J. Am. Chem. Soc. 126*, 7281–7292.

25. Laskowski, R. A., Rullmannn, J. A., MacArthur, M. W., Kaptein, R., and Thornton, J. M. (1996) AQUA and PROCHECK-NMR: Programs for checking the quality of protein structures solved by NMR. *J. Biomol. NMR 8*, 477–486.

26. Morales-Ríos, M. S., García-Martínez, C., Joseph-Nathan, P., and Zepeda, L. G. (1995) ^{35}Cl/^{37}Cl one-bond isotope effects on ^{13}C chemical shifts in a series of para-substituted chlorobenzenes. *Magn. Reson. Chem. 33*, 149–151.

27. Silverstein, R. M., Bassler, G. C., and Morrill, T. C. (1991) Spectrometric identification of organic compounds , 5th ed., p 248, Wiley, New York.

28. Levitt, M. H. (2001) Spin dynamics: Basics of nuclear magnetic resonance , John Wiley & Sons, Chichester, U.K.

29. Hooft, R. W., Vriend, G., Sander, C., and Abola, E. E. (1996) Errors in protein structures. *Nature 381*, 272.

30. Nederveen, A. J., Doreleijers, J. F., Vranken, W., Miller, Z., Spronk, C. A. E. M., Nabuurs, S. B., Guntert, P., Livny, M., Markley, J. L., Nilges, M., Ulrich, E. L., Kaptein, R., and Bonvin, A. M. J. J. (2005) RECOORD: A recalculated coordinate database of 500+ proteins from the PDB using restraints from the BioMagResBank. *Proteins 4*, 662–672.

31. Takeda, S., Yamashita, A., Maeda, K., and Maeda, Y. (2003) Structure of the core domain of human cardiac troponin in the Ca^{2+}-saturated form. *Nature 424*, 35–41.

32. Bonvin, A. M. J. J., and Brunger, A. T. (1995) Conformational variability of solution nuclear magnetic resonance structures. *J. Mol. Biol. 250*, 80–93.

33. Paakkonen, K., Annila, A., Sorsa, T., Pollesello, P., Tilgmann, C., Kilpelainen, I., Karisola, P., Ulmanen, I., and Drakenberg, T. (1998) Solution structure and main chain dynamics of the regulatory domain (residues 1–91) of human cardiac troponin C. *J. Biol. Chem. 273*, 15633–15638.

34. Rieping, W., Habeck, M., and Nilges, M. (2005) Inferential structure determination. *Science 309*, 303–306.

35. Habeck, M., Rieping, W., and Nilges, M. (2006) Weighting of experimental evidence in macromolecular structure determination. *Proc. Natl. Acad. Sci. U.S.A. 6*, 1756–1761.

36. Gagné, S. M., Tsuda, S., Li, M. X., Smillie, L. B., and Sykes, B. D. (1995) Structures of the troponin C regulatory domains in the apo and calcium-saturated states. *Nat. Struct. Biol. 2*, 784–789.

37. Herzberg, O., Moult, J., and James, M. N. G. (1986) A model for the Ca^{2+}-induced conformational transition of troponin C. A trigger for muscle contraction. *J. Biol. Chem. 261*, 2638–2644.

38. Gagné, S. M., Li, M. X., and Sykes, B. D. (1997) Mechanism of direct coupling between binding and induced structural change in regulatory calcium binding proteins. *Biochemistry 36*, 4386–4392.

39. Paakkonen, K., Sorsa, T., Drakenberg, T., Pollesello, P., Tilgmann, C., Permi, P., Heikkinen, S., Kilpelainen, I., and Annila, A. (2000) Conformations of the regulatory domain of cardiac troponin C examined by residual dipolar couplings. *Eur. J. Biochem. 267*, 6665–6672.

40. Eichmuller, C., and Skrynnikov, N. R. (2007) Observation of microsecond time-scale protein dynamics in the presence of Ln^{3+} ions: Application to the N-terminal domain of cardiac troponin C. *J. Biomol. NMR 37*, 79–95.

41. Tanaka, T., Ohmura, T., and Hidaka, H. (1982) Hydrophobic interaction of the Ca^{2+}-calmodulin complex with calmodulin antagonists. Naphthalenesulfonamide derivatives. *Mol. Pharmacol. 22*, 403–407.

42. Lindhout, D. A., Boyko, R. F., Corson, D. C., Li, M. X., and Sykes, B. D. (2005) The role of electrostatics in the interaction of the inhibitory region of troponin I with troponin C. *Biochemistry 44* (45), 14750–14759.

43. Schwieters, C. D., Kuszewski, J. J., Tjandra, N., and Clore, G. M. (2003) The Xplor-NIH NMR molecular structure determination package. *J. Magn. Reson. 160*, 65–73.